nature | methods

A bright and photostable photoconvertible fluorescent protein

Sean A McKinney, Christopher S Murphy, Kristin L Hazelwood, Michael W Davidson & Loren L Looger

Supplementary figures and text:

Supplementary Figure 1	Comparison of fusions with Dendra2, mEos2 and tdEos.
Supplementary Figure 2	Sequence alignment of wtEos, mEos2 and Dronpa.
Supplementary Figure 3	Absorbance, excitation and emission spectra of mEos2.
Supplementary Figure 4	pH dependence of mEos2 spectra.
Supplementary Figure 5	mEos2 maturation at 37°C.
Supplementary Figure 6	Contrast ratio of mEos2, tdEos and Dendra2.
Supplementary Figure 7	Gel filtration analysis of dEos, mEos and mEos2.
Supplementary Figure 8	Fluorescence polarization measurements.
Supplementary Figure 9	Monomeric Eos variants show poor photoactivation.
Supplementary Figure 10	Fluorescence imaging of mEos2 fusion vectors.
Supplementary Figure 11	Photobleaching kinetics of optical highlighter FPs.
Supplementary Figure 12	Single molecule localization precision of mEos2 and Dendra2.
Supplementary Figure 13	Dependence of single molecule localization precisions of mEos2 on intensity and exposure time.
Supplementary Table 1	Dronpa-based mutations tested on mEos.
Supplementary Table 2	Photon statistics and localization precisions of commonly used super-resolution probes.
Supplementary Methods	

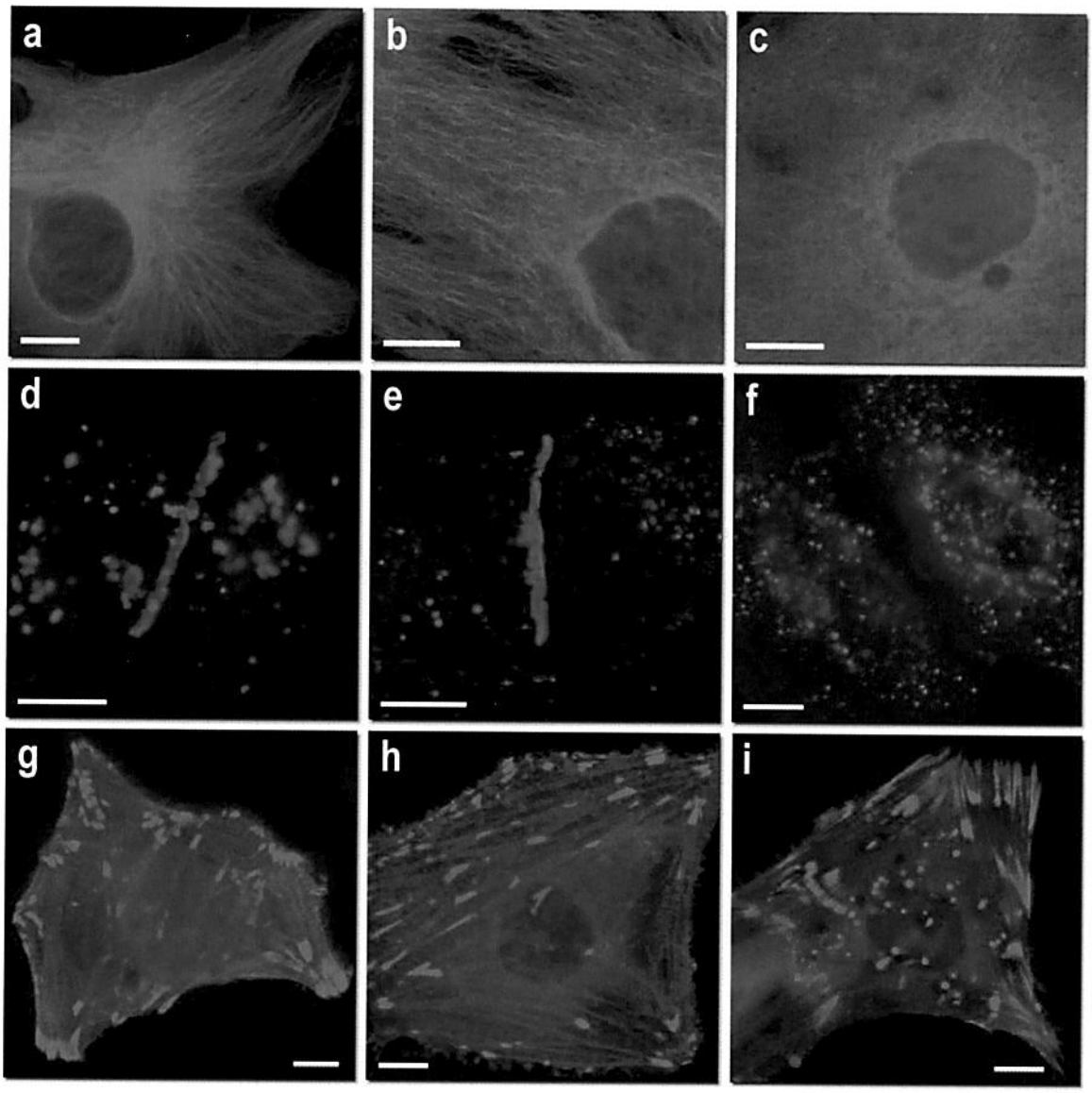

Supplementary Figure 1. Comparison of fusions with Dendra2, mEos2, and tdEos (**a-c**) fusions to human α-tubulin with (**a**) Dendra2, (**b**) mEos2, and (**c**) tdEos; (**d-f**) fusions to rat α-1 connexin 43 with (**d**) Dendra2, (**e**) mEos2, and (**f**) tdEos; (**g-i**) fusions to mouse vasodilator-stimulated phosphoprotein (VASP) with (**g**) Dendra2, (**h**) mEos2, and (**i**) tdEos. Note the normal localization patterns for all fusions with Dendra2 and mEos2, which are similar to those observed with mEGFP. In contrast, tdEos exhibits punctate labeling with α-tubulin (**c**), lack of gap junction plaque formation (**f**), and numerous cytoplasmic aggregates with VASP (**i**).

Nature Methods: doi:10.1038/nmeth.1296

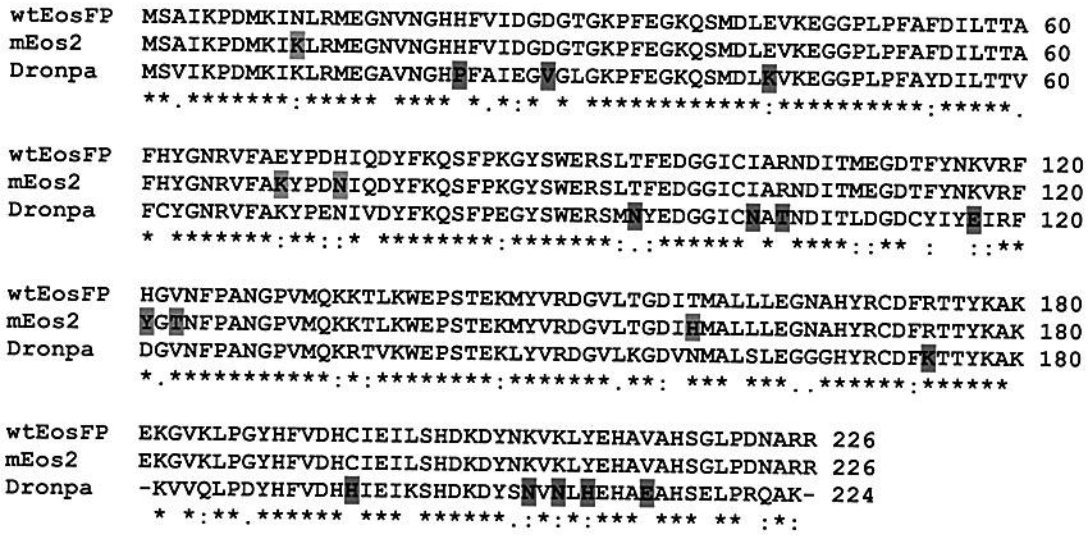

Supplementary Figure 2. Sequence alignment of wtEosFP, mEos2 and Dronpa

Mutations from wtEosFP to mEos2 are marked in green and red. Red mutations were already added to make dEos (T158H) and mEos (V123T and T158H), or were random mutations (H121Y). Green and blue mutations were guided from Dronpa. Blue mutations showed no 37° C improvement while green did.

Nature Methods: doi:10.1038/nmeth.1296

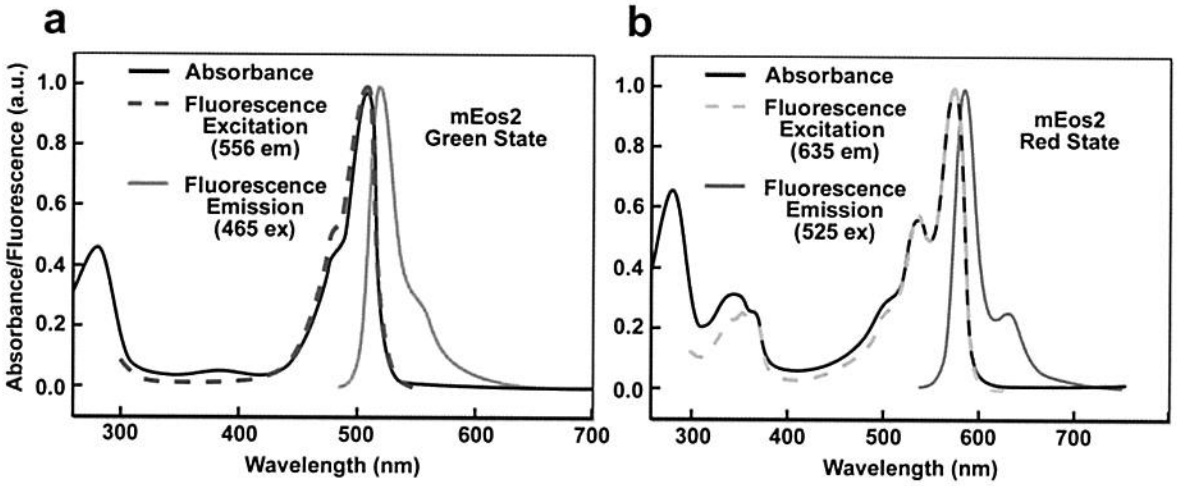

Supplementary Figure 3. Absorbance, Excitation, and Emission Spectra of mEos2

(**a**) The absorbance, excitation and fluorescence emission spectral profiles of native (green species) mEos2 display maxima at 506 nm and 519 nm, respectively. (**b**) The red (photoconverted) species of mEos2 exhibits spectral profiles that have maxima at 573 nm and 584 nm, respectively. The green form of m2Eos is as efficiently converted as tdEos[1] which is critical for performing current serial two-color PALM experiments[2]. Both the red and green forms of dEos and mEos2 have a minority population that can be turned dark and re-stimulated by 405nm (much like Dronpa). Some mutants with known Dronpa mutations make this feature more pronounced. As it is largely a minority, this feature should not prove disadvantageous but it should be borne in mind by those attempting single molecule counting using PALM-like applications.

Nature Methods: doi:10.1038/nmeth.1296

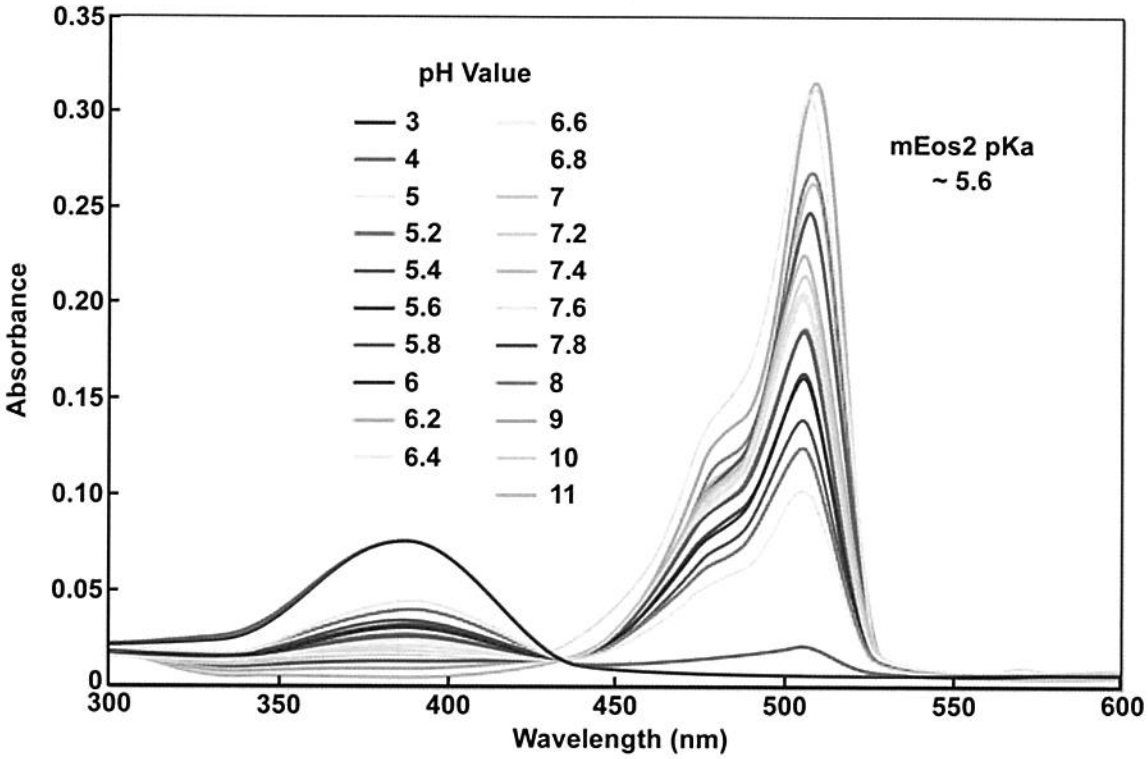

Supplementary Figure 4. pH Dependence of mEos2 Spectra

Decreased pH values increase the 395 nm peak amplitude while decreasing the maximum absorbance at 490 nm. Similar to the parent FPs: wtEosFP, dEos, and tdEos, the pKa of mEos2 is ~5.6[1].

Nature Methods: doi:10.1038/nmeth.1296

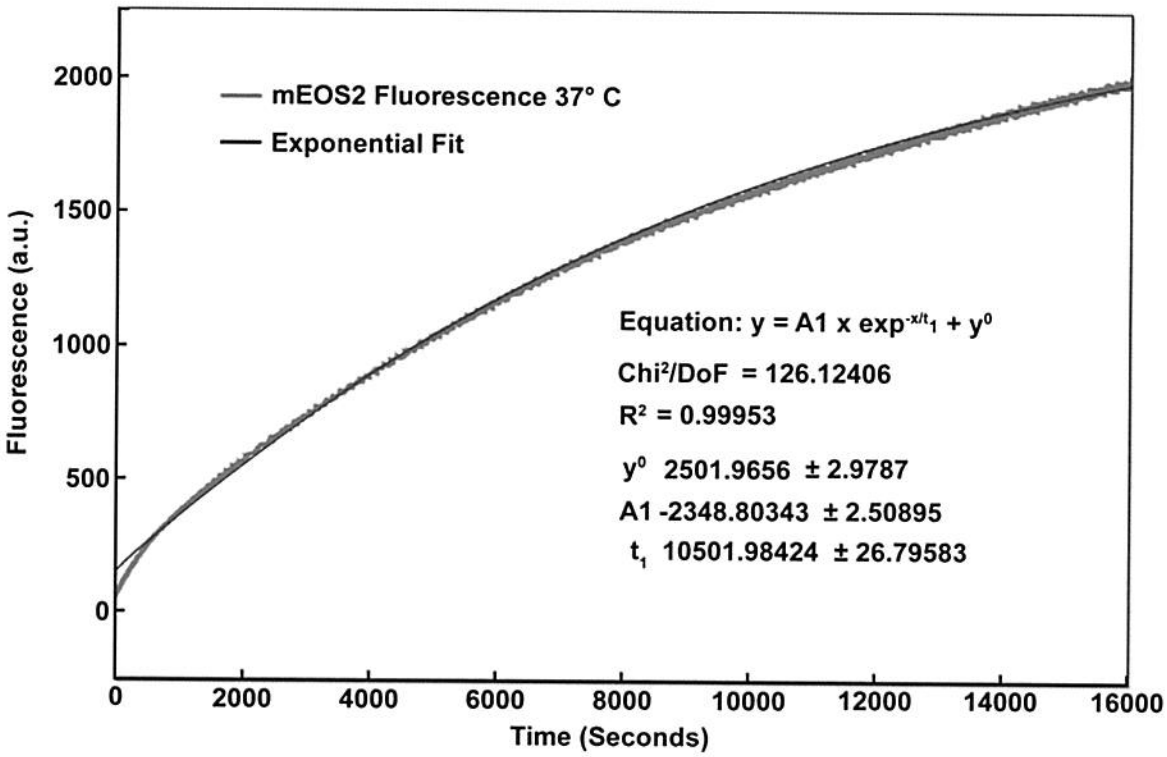

Supplementary Figure 5. mEos2 maturation at 37° C

The mEos2 maturation profile fits a single exponential curve with a time constant of 10,500 s, which corresponds to a $t_{1/2}$ for maturation of approximately 2 hrs. In comparison, Dendra2 was found to have an identical ~2 hr maturation time (data not shown), and wtEosFP has been reported[1] to mature in ~1.2 hr in *Escherichia coli*.

Nature Methods: doi:10.1038/nmeth.1296

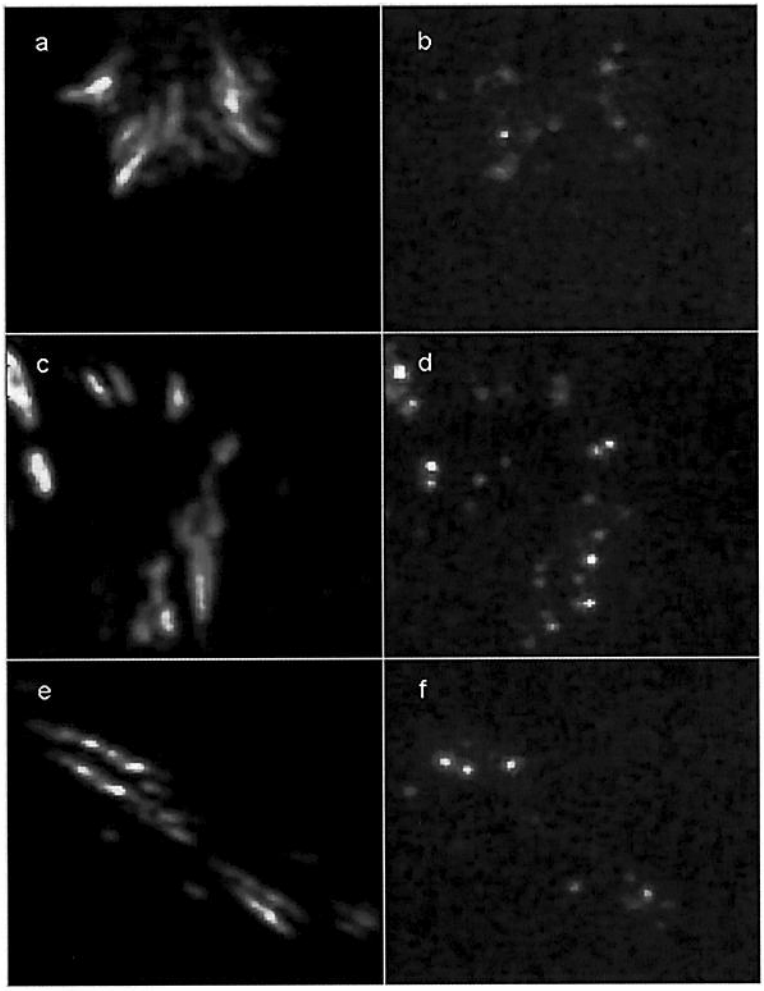

Supplementary Figure 6. Contrast ratio of mEos2, tdEos, and Dendra2

Dendra2 (**a-b**), tdEos (**c-d**) and mEos2 (**e-f**) all have comparably excellent contrast ratios. Panels on the left (**a, c, e**) are TIRF images of the red forms of each species fused to zyxin in HeLa cells. Panels on the right (**b, d, f**) are individual frames acquired early in a PALM stack, showing individual molecules clearly resolvable against an almost non-existent background of unconverted molecules. All three constructs exhibited the same level of background per pixel per frame in pixels that did not have a molecule turned on in them (data not shown).

Nature Methods: doi:10.1038/nmeth.1296

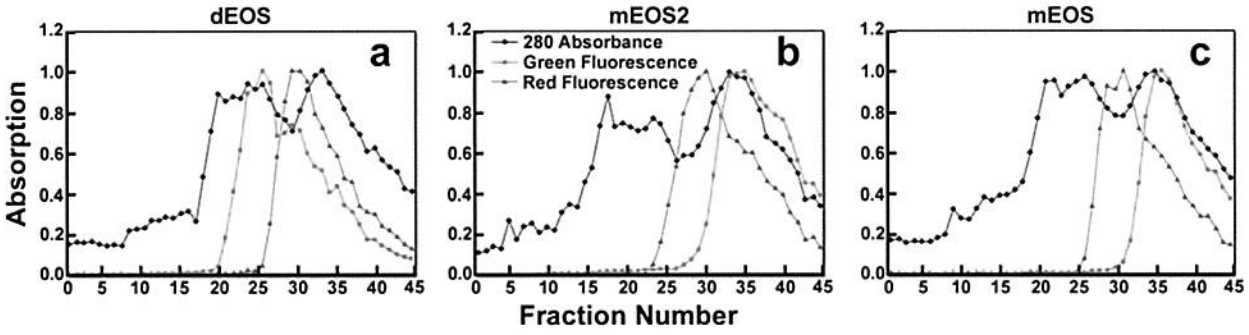

Supplementary Figure 7. Gel filtration analysis of dEos, mEos, and mEos2

Carbonic anhydrase (MW 29,000), ovalbumin (MW 43,000), conalbumin (MW 75,000) and mCherry (MW 27,000) were run simultaneously on a gel filtration column with the FP optical highlighter listed above each graph. Fractions were collected in a microplate and UV absorbance, green fluorescence (480/515), and red fluorescence (560/580) were monitored. mCherry (red) fluorescence is always observed to fall between the merged ovalbumin/conalbumin peak and the lighter carbonic anhydrase peak. In contrast, dEos (green fluorescence) elutes at the same point as ovalbumin and is clearly of higher molecular weight than mCherry (**a**). Both the original mEos and mEos2 (green fluorescence) elute at the same point as carbonic anhydrase and are clearly lower in apparent molecular weight than mCherry (**b** and **c**).

Nature Methods: doi:10.1038/nmeth.1296

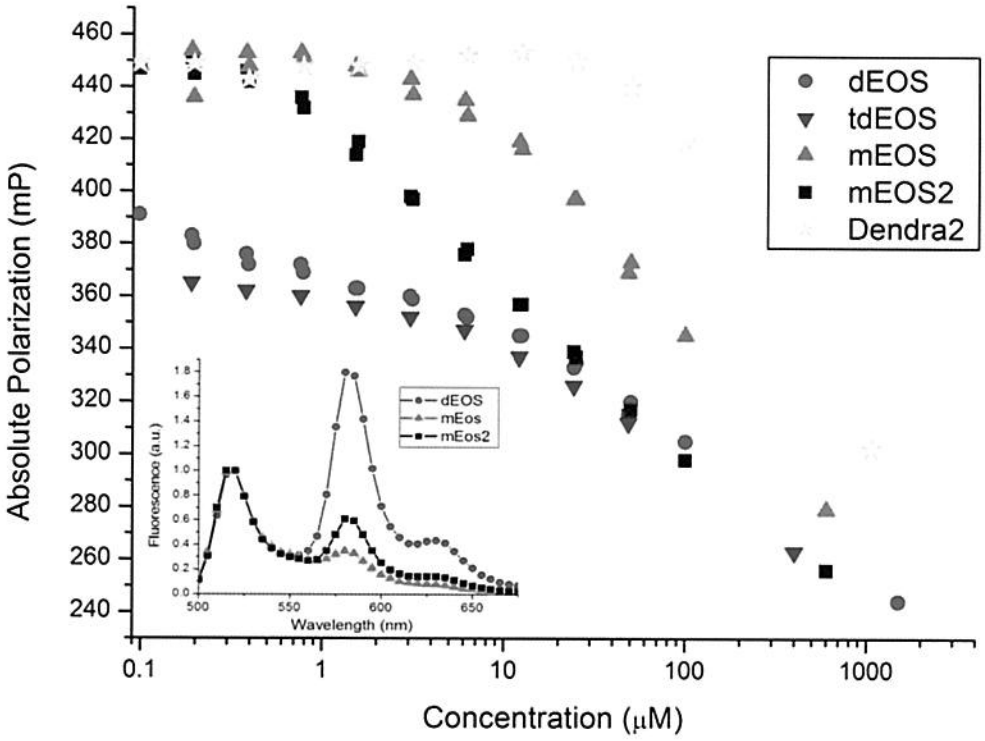

Supplementary Figure 8. Fluorescence polarization measurements

Fluorescence polarization indicates that mEos, mEos2, and Dendra2 form dimers at high concentrations, which is consistent with size exclusion chromatography measurements[1,3]. mEos2 forms a level of dimeric character equivalent to dEos at approximately a 4-5 times lower molar concentration than mEos. As monomers aggregate into dimers, energy transfer begins to occur, depolarizing the emission signal. **Inset:** half-photoconverted (506:573 absorbance ratio of 1:1) highlighter dimerization at a concentration of 3μM for dEos, mEos, and mEos2. The probes demonstrate varying degrees of energy transfer, with mEos exhibiting little if any transfer, mEos2 exhibiting slightly more, and dEos exhibiting a large amount.

Nature Methods: doi:10.1038/nmeth.1296

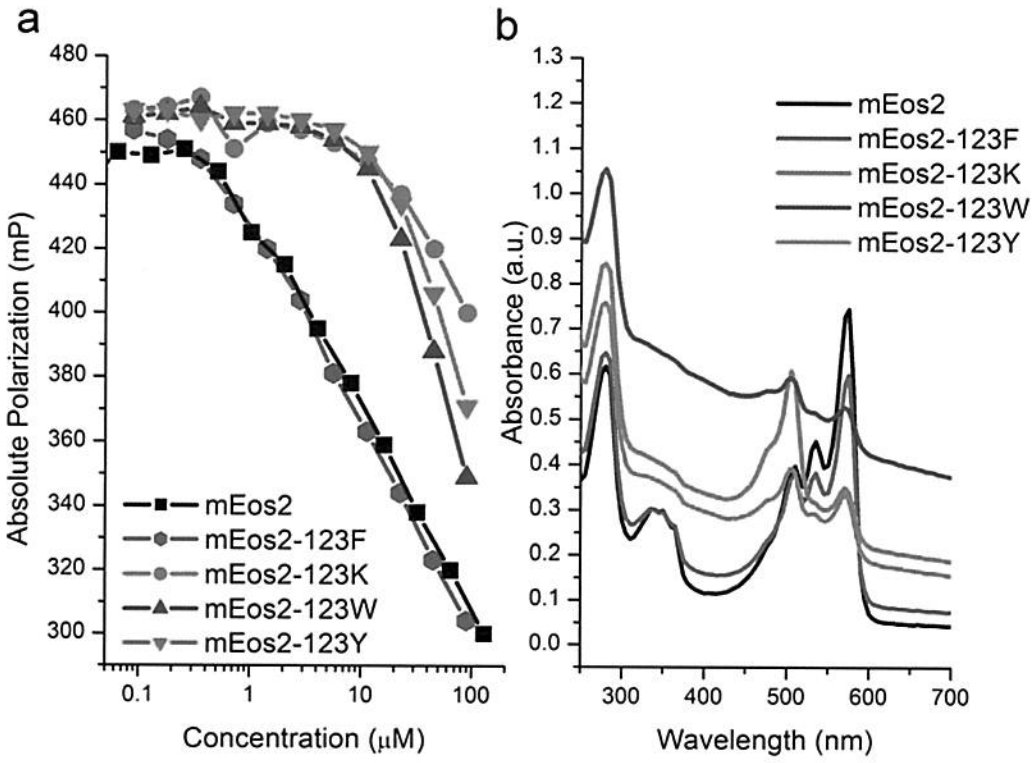

Supplementary Figure 9. Monomeric Eos variants show poor photoactivation

Polarization measurements suggest that several mutations of mEos2 at T123 result in less dimerization at higher concentrations (**a**). However similar concentrations of these variants fail to photoactivate completely as evinced in absorbance measurements following 405nm irradiation (**b**). They form cloudy solutions to the eye and in absorbance measurements, where a constantly decaying linear scattering component is present.

Nature Methods: doi:10.1038/nmeth.1296

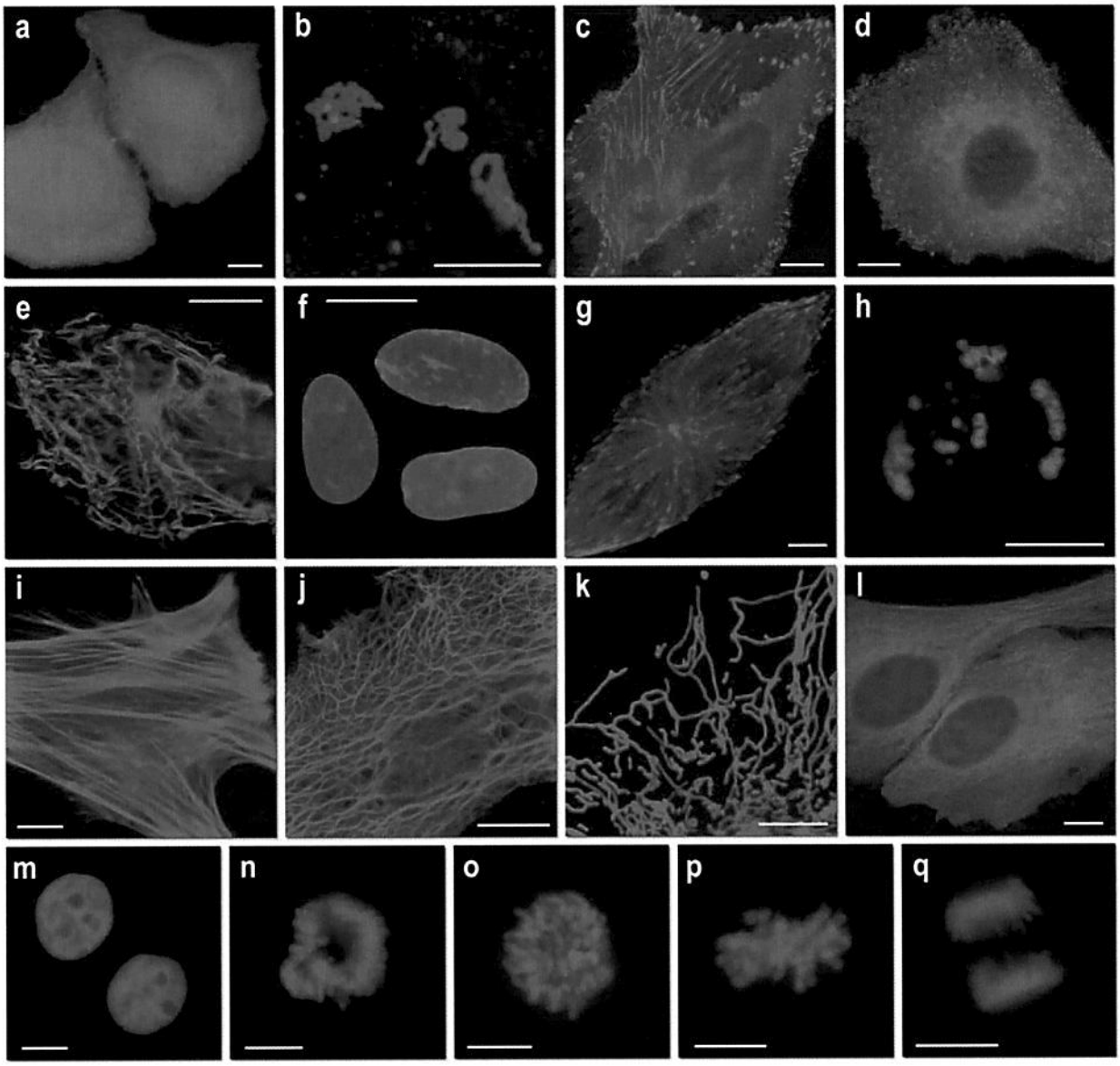

Supplementary Figure 10

Nature Methods: doi:10.1038/nmeth.1296

Supplementary Figure 10. Fluorescence imaging of mEos2 fusion vectors

(**a**) mEos2-N1 cloning vector expressed in HeLa cells is found in both the cytoplasm and nucleus with no specific localization. (**d**, **f**, **i**, **l**) mEos2 C-terminal fusion constructs; for each fusion protein the linker amino acid length is indicated after the name of the targeted organelle or fusion protein: (**d**) mEos2-clathrin light chain-15 (human); (**f**) mEos2-lamin B1-10 (human); (**i**) mEos2-β-actin-7 (human); (**l**) mEos2-α-tubulin-6 (human); (**b**, **c**, **e**, **g**, **h**, **j**, **k**) mEos2 N-terminal fusion constructs; (**b**) mEos2-Cx43-7 (rat); (**c**) mEos2-paxillin-22 (chicken); (**e**) mEos2-vimentin-7 (human); (**g**) mEos2-EB3-7 (human microtubule-associated protein; RP/EB family); (**h**) mEos2-golgi-7 (N-terminal 81 amino acids of human β-1,4-galactosyltransferase); (**j**) mEos2-keratin-17 (human cytokeratin 18); (**k**) mEos2-mitochondria-7 (human cytochrome C oxidase subunit VIII). (**m**)-(**q**) Images of a single HeLa cell expressing mEos2-H2B-6 (N-terminus; human) progressing through prophase (**m**), prometaphase (**n**), metaphase (**o**), anaphase (**p**) and interphase (**q**), respectively. The cell line used for expressing mEos2 fusion vectors was gray fox lung fibroblast cells (FoLu) in panels (**g**), (**i**), and (**l**) and human cervical adenocarcinoma cells (HeLa) in the remaining panels. Scale bars represent 10 μm.

Nature Methods: doi:10.1038/nmeth.1296

Supplementary Figure 11

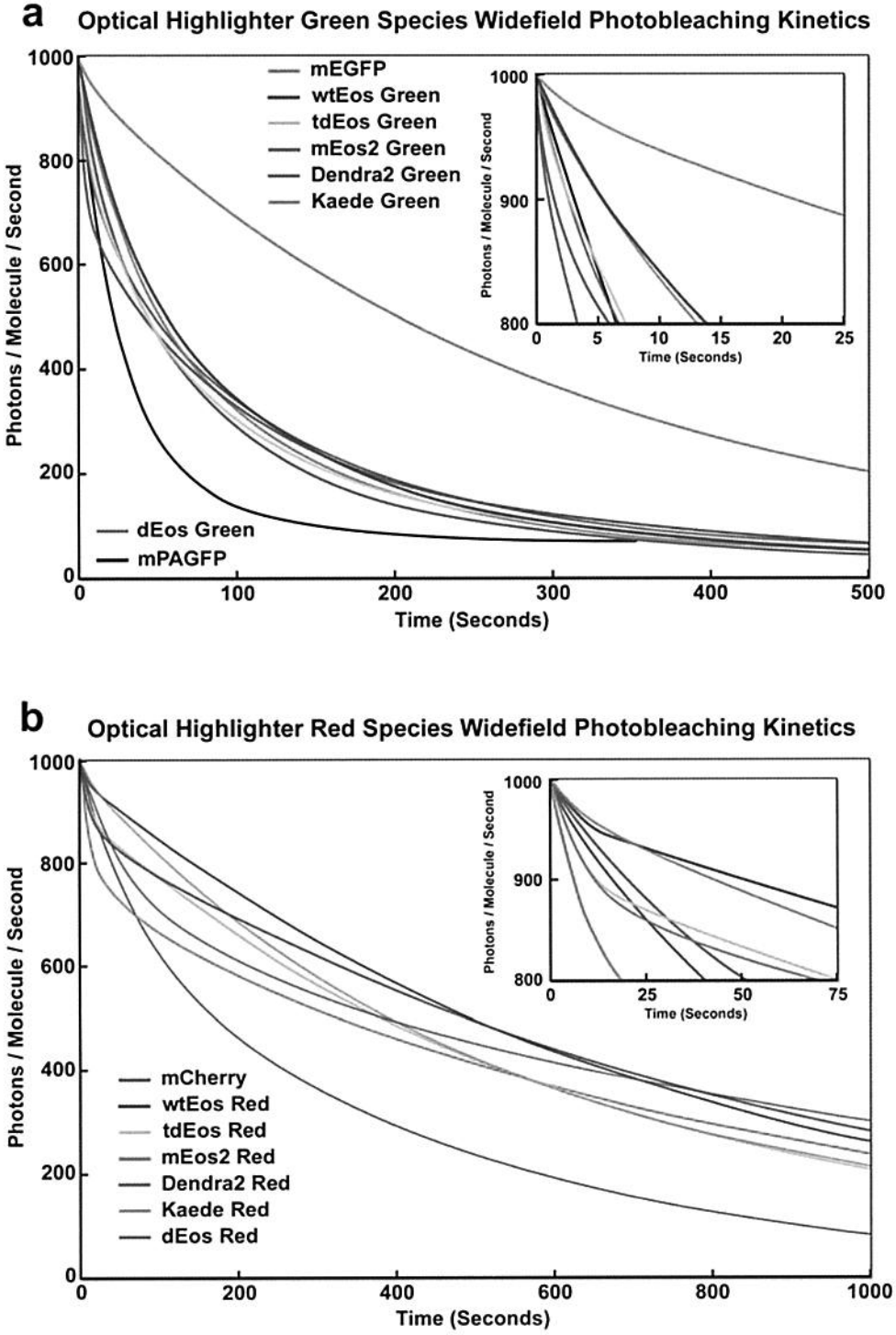

Nature Methods: doi:10.1038/nmeth.1296

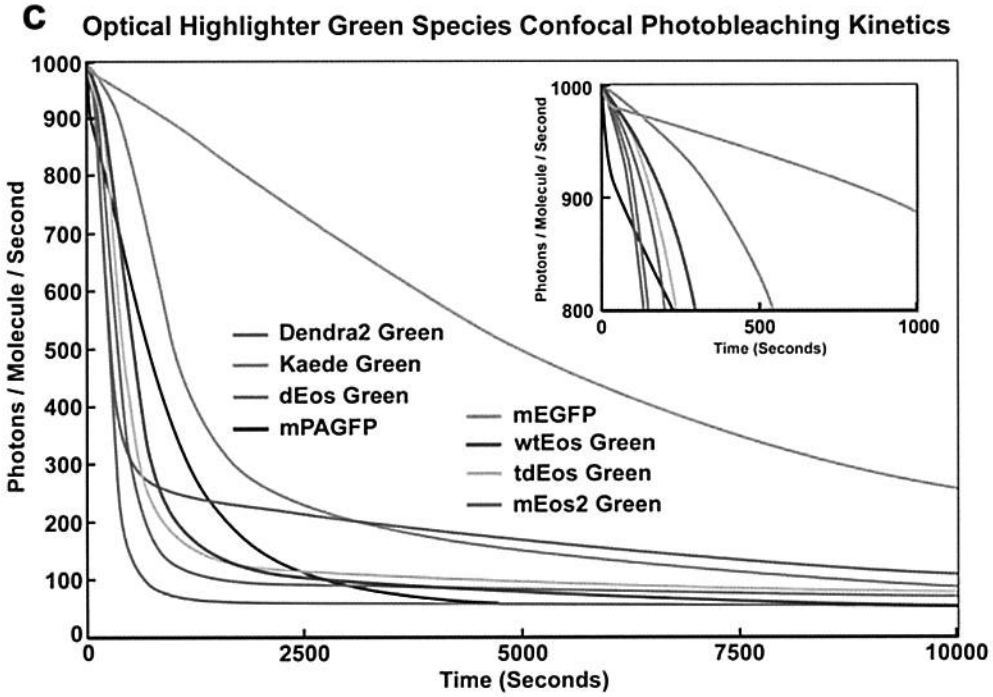

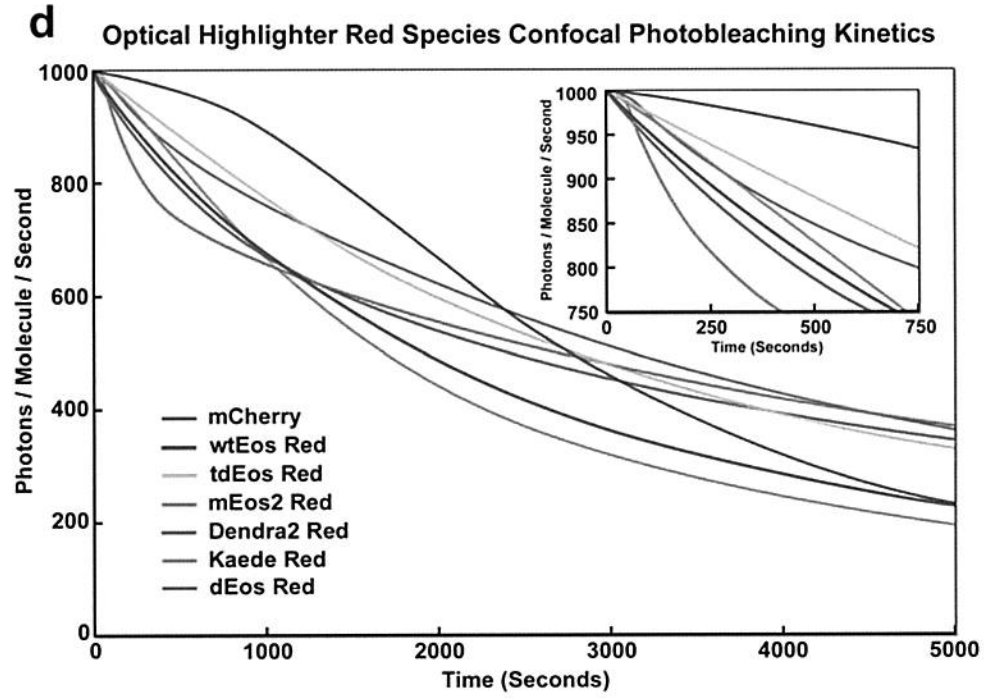

Nature Methods: doi:10.1038/nmeth.1296

Supplementary Figure 11. Photobleaching kinetics of optical highlighter FPs

Fluorescence intensity is plotted versus normalized total exposure time with an initial emission rate of 1,000 photons/sec/molecule for all curves (**a-d**), whereas the x-axis is the normalized total imaging time. Samples are mEGFP, mCherry, mPA-GFP, wtEosFP, dEos, tdEos, mEos2, Dendra2, and Kaede FPs fused to human histone H2B and expressed in living HeLa cells. (**a**) Wide-field microscopy (metal halide illumination) photobleaching curves for mEGFP, mPA-GFP and the Eos/Dendra2 native (green) species. (**b**) Wide-field photobleaching curves for mCherry and the photoconverted (red) species of the same highlighters as in (**a**). (**c**) Confocal laser scanning microscopy photobleaching curves for mEGFP, mPA-GFP, and the green species of Eos and Dendra2. (**d**) Confocal photobleaching curves for mCherry and the red species of the same highlighters as in (**c**).

Nature Methods: doi:10.1038/nmeth.1296

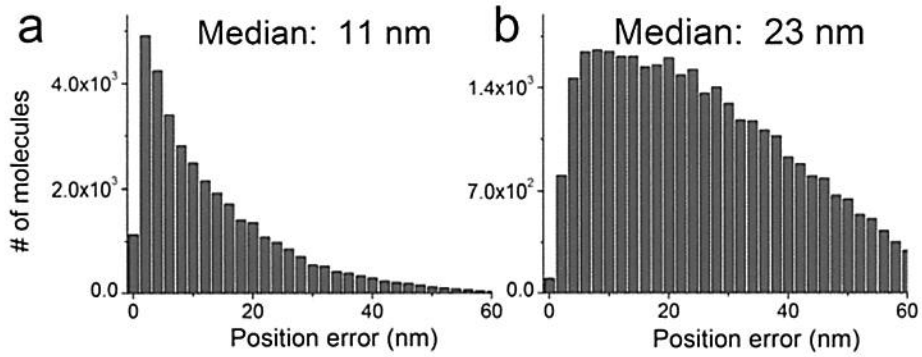

Supplementary Figure 12. Single molecule localization precision of mEos2 and Dendra2

One-dimensional localization error histograms track localization precision based on the signal and background photons observed for each molecule. Statistics on fixed HeLa cells expressing (**a**) mEos2-Keratin and (**b**) Dendra2-Keratin show a factor of two difference in resolving power. Note that due to the statistical nature of analyzing one molecule at a time, one can in fact arbitrarily select a precision level and then filter out all molecules below that localization precision. However, there are two ceilings for determining the final resolution achievable by a probe. One is the localization precision (determined by signal photons and background noise) and the other is the Nyquist criterion, which for PALM-like applications requires the spacing of molecules to be twice as small as the desired resolution. In the case of unlimited molecular densities this would not be a problem, as one could choose the resolution to any precision by selecting to image only those molecules whose localizations were known with that precision. However, single molecule densities here and reported previously range typically from thousands to hundreds of thousands per square micron, corresponding to a range of 2D maximum Nyquist resolutions of 6-48nm. Since the typical Nyquist resolution is very close to the localization precision, and the Nyquist resolution depends on the total number of molecules, sacrificing poorly localized Dendra2 molecules has almost no net benefit on the final resolution of the image.

Nature Methods: doi:10.1038/nmeth.1296

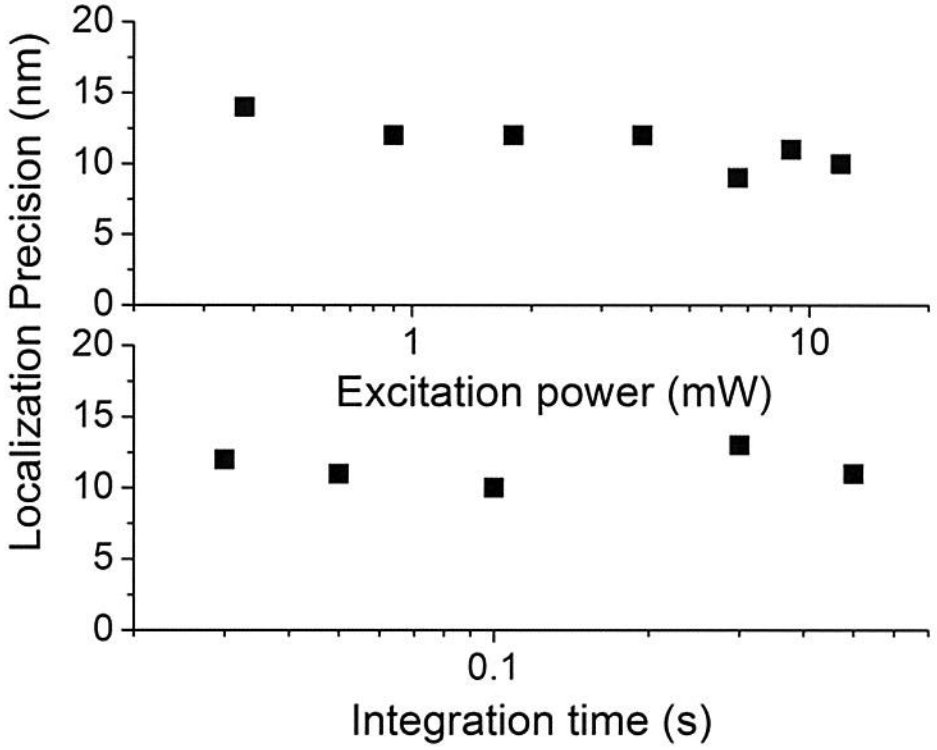

Supplementary Figure 13. Dependence of single molecule localization precisions of mEos2 on intensity and exposure time

One-dimensional localization error histograms show that for the power ranges used there are consistent localization precisions. (Dendra2 has a similar power profile averaging 22nm). Data were taken on purified protein molecules in 1.5% agarose[4].

Nature Methods: doi:10.1038/nmeth.1296

Position	mEos	Dronpa	Structure	Result	Rationale for position selection
11	Asn	Lys	β strand	Brighter	Better strand preference. May improve electrostatics.
22	His	Pro	β strand	NI	May improve strand stability; pos22 is in "proline"-compatible phi-psi range
28	Asp	Val	β strand	NI	Better strand preference.
43	Glu	Lys	β strand	NI	Better strand preference. May improve electrostatics.
70	Glu	Lys	β strand	Brighter	Better strand preference. May improve electrostatics.
74	His	Asn	β_1 turn	Brighter	Better turn preference.
94	Thr	Asn	β strand	NI	May improve monomericity by interaction across dimer-dimer interface
96	Glu	Arg	β_1 turn	NI	May improve electrostatics.
102	Ile	Asn	β strand	NI	May improve monomericity by interaction across dimer-dimer interface
104	Arg	Thr	β strand	NI	Better strand preference. May improve electrostatics.
117	Lys	Glu	β strand	NI	May improve electrostatics.
121	His	Asp	β strand	NI	May improve electrostatics. May strongly disfavor dimer-dimer interaction.
121	His	Tyr	β strand	Brighter	Single base mutation (TAT) relative to target Asp (GAT). Better strand preference.
158	His	Arg	β strand	NI	Better strand preference. May improve electrostatics.
174	Arg	Lys	β strand	NI	May improve electrostatics.
191	Phe	Tyr	β strand	NI	Better strand preference.
195	Cys	His	β strand	NI	Removes potential aggregation site.
207	Lys	Asn	β strand	NI	May improve electrostatics.
209	Lys	Asn	β strand	NI	May improve electrostatics.
211	Tyr	His	β strand	NI	May improve surface hydrogen bonding
215	Val	Glu	β strand	NI	May improve electrostatics.

Supplementary Table 1. Dronpa-based mutations tested on mEos. Protein positions were selected based on differences in the Dronpa and Eos sequences. Amino acid substitutions with better secondary structure preference[5] were more likely to assist folding and maturation at 37C.

Supplementary Table 2

Fluorophore	N_p, typical detected photons per burst	Reported localization (σ,nm) 1D[a]	Density obtained (μm^{-2})[b]	Ref
Synthetic Dyes				
Cy5	6000	3 (56)		[6]
Cy7	1000	9		[6]
Fluorescent Proteins				
paGFP		41 (40)	6900**[7]	[7]
Dronpa	120	26	4500	[2]
rsFastLime	50	(50)	NA	[8]
PS-CFP2	260	27	5600	[6]
psCherry		(75)	NA	[9]
tdEos	490	10	13000	[2]
Dendra2	131	23	8400	
mEos2	360	11 (50)	7900	

[a]Numbers in parentheses indicate the smallest feature resolved with the probe, and do not necessarily reflect the probe's maximum localization precision.

[b]Numbers acquired by our laboratory on zyxin fusions in fixed HeLa cells 24 hrs after transfection except for paGFP, which is taken from literature.

Supplementary Table 2. Photon statistics and localization precisions of commonly used super-resolution probes. All data were taken when labeling biological samples. With the exception of rsFastLime and psCherry, all localization precisions are derived from the typical photon budget ($\mathbf{N_p}$), the background noise (**b**), and the system point-spread function and pixel size[10]. For a variety of applications, as in examining the width of a one-dimensional fiber, 1D precision is more appropriate in determining the limiting resolution. Together with the probe's molecular density, localization precision determines that probe's maximum resolution in STORM or PALM-like applications. For comparing the fluorescent protein probes we provide the maximum probe density obtained for a consistent but arbitrary choice of parameters (with the exception of paGFP as provided by literature). These numbers are provided for a rough comparison of probes' maximum density only, not as an absolute limit on probe density, which varies with construct, transfection conditions, growing conditions, cell line, cell and even region

Nature Methods: doi:10.1038/nmeth.1296

of the cell. Densities are largely consistent with the exception of tdEos and Dronpa. tdEos is particularly high in density, probably as the result of having two copies of the Eos for every copy of the partner. Dronpa is particularly low in density, likely the result of a significantly smaller photon budget making shorter bursts indistinguishable from noise.

Nature Methods: doi:10.1038/nmeth.1296

Supplementary Methods

Molecular modeling and mutant design. We pursued a strategy of side-chain grafting to stabilize the existing monomeric Eos variant (wtEosFP with V123T, T158H). EosFP is highly homologous to the green reversibly photoactivatable protein Dronpa, which is bright, monomeric, and matures well at 37 °C. A structural alignment of EosFP (PDB 1ZUX) and Dronpa (PDB 2IE2) was created to identify divergent positions at which the Dronpa side-chain may contribute to thermal stability and monomeric character. To avoid disturbing the chromophore environment, our first approach was to mutate only sites on the barrel exterior, with an emphasis on positions where introducing a Dronpa residue might improve secondary structure preference or electrostatics (**Supplementary Table 1**), thus stabilizing the entire protein. Twenty positions were selected for mutagenesis, and three mutations (N11K, E70K, H74N) were found to rescue fluorescence at 37° C in bacterial colonies. Surprisingly, these mutations are not found at either dimer-dimer interface and are solvent-exposed in the tetrameric crystal structure. All three mutations are predicted to improve secondary structure preference (11, 70: β-strand; 74: Type I β-turn), and the mutations N11K and E70K may additionally improve electrostatics. Serendipitous mutation of His121 (the center of the A-C dimer-dimer interface) to Tyr rather than to the primer-encoded mutation Asp also aided 37 °C folding, potentially by simultaneously optimizing β-strand preference and disfavoring dimerization. These four mutations (dubbed mEos2) turned the original mEos into a functional green-to-red photoconvertible fluorescent protein at 37° C (**Supplementary Fig. 2**).

Plasmid construction. Synthetic DNA oligonucleotides for cloning and library construction were purchased from Integrated DNA Technologies. PCR products and

Nature Methods: doi:10.1038/nmeth.1296

products of restriction digests were purified by gel electrophoresis and extracted using the QIAquick™ gel extraction kit. Plasmid DNA was purified from overnight cultures by using QIAprep Spin Miniprep kit (QIAGEN). Restriction endonucleases and T4 DNA ligase were purchased from either Invitrogen or New England Biolabs. Mammalian expression vector DNA sequencing reactions were analyzed at the Florida State University Bioanalytical and Molecular Cloning DNA Sequencing Laboratory.

Bacterial Expression Vectors, Mutagenesis and Protein Expression/Purification. All fluorescent proteins were inserted into the pRSETA vector (Invitrogen) using BamHI and EcoRI (tEos, dEos, mEos made by George Patterson, NIH). tdEos was made from dEos first by removing the natural HindIII site and replacing the stop codon with glycine. Next a PCR produced second copy of dEos with a 12 amino acid linker between EcoRI and HindIII was inserted into the same vector. Mutagenesis to generate new mEos mutants was performed by Kunkel mutagenesis[11]. Colonies were screened on a fluorescence dissecting scope (Olympus). Interesting mutants were picked, grown, plasmid isolated and sequenced (Janelia Farm Molecular Biology Shared Resource). For protein over-expression, plasmid was transformed into BL21(DE3)pLysS (Novagen), plated, colonies picked and grown to 0.6OD in 400mL 2YT growth media with antibiotics, shaking at 37C. Cultures were then induced with 1mM IPTG and moved to room temperature shaking for 24-48 hrs. Pellets were harvested, frozen at -20C overnight or longer, and thawed. They were then resuspended in IMAC A buffer (100mM $Na_xH_xPO_4$ pH 7.4, 1M NaCl) with 1mg/mL lysozyme (Sigma Aldrich) and incubated on ice for at least 30 min. The suspension was sonicated and centrifuged at 8000g for 10 minutes. The supernatant was spun again at 35,000g for ~1 hr before being filtered and loaded onto an IMAC (GE

Nature Methods: doi:10.1038/nmeth.1296

Healthcare) column loaded with $NiCl_2$. Gradient purification was performed using the BioLogic LP (BioRad) with elution buffer (IMAC A plus 300mM imidazole); fluorescent fractions were pooled and buffer exchanged with Amicon Ultra centrifuge membranes into PBS (Millipore).

HeLa Cell Transfection and Fixation. HeLa cells (ATCC, CCL-2) passages JFRC+4-JFRC+15 were grown in EMEM containing 10% FBS to ~55-85% confluency. Trypsinized cells were then transiently transfected at ~$\underline{1\text{-}8X10^5}$ cells per shuttle well with a Nucleofector 96-well shuttle system (Amaxa Biosystems) using Cell Line Nucleofector Kit SE, program CN-114, and 0.5-1.0μg plasmid DNA per shuttle well. Cells were fixed incubating with 2% *para*-formaldehyde in PHEM (60mM Pipes, 25mM HEPES, 10mM EGTA, and 2mM MgCl2, pH 6.9) for 15 minutes and washing 3X with PHEM.

PALM Imaging. PALM imaging of mEos2 and Dendra2 was performed as described previously for imaging tdEos[2], including the FF562-Di02-25x36 dichroic mirror and FF01-617/73-25 emission filter from Semrock for fluorescence imaging. For comparative single molecule localization measurements, purified protein was mixed with warm 1.5% agarose in PBS and added to a high refractive index coverslip (Olympus), incubated to allow agarose to solidify, and imaged using a 1.65NA 100X objective in an IX81 microscope. For fixed cell imaging, samples were prepared on high refractive index coverslips and imaged the same way. To remove sample drift for keratin and EB3 images, 100nm gold beads were diluted 10X in PHEM and applied to the coverslip for several minutes before being removed and rinsed with PHEM. Data analysis and image construction including peak finding, localization, dark state removal and photophysical analysis was performed as previously described[12]. Transient dark states were considered

Nature Methods: doi:10.1038/nmeth.1296

to have occurred where any two molecules localizing to the same pixel but separated in time by fewer than 0.5s. For comparing molecular densities, zyxin fusions transfected in HeLa cells using Nucleofector and fixed after 24 hrs. The brightest cells were imaged and the most dense 130nmX130nm region was determined.

Spectroscopic, Oligomeric and Maturation Characterization. All absorbance spectra, fluorescence spectra and fluorescence polarization data were obtained in a Safire^2 (Tecan) with UVStar 96 well plates (Greiner). Quantum yields were measured compared to fluorescein in 0.1M NaOH (green form Eos) and Cresyl Violet in methanol (red form Eos). As our values for the green form extinction coefficient differed significantly from those published for tEos and dEos[1], we performed concentration measurements averaged with four different assays (BCA, Bradford, 280 absorbance, and the Agilent 2100 Bioanalyzer). To perform photoconversions, either a 405-nm laser (Coherent Cube) was used on individual wells of a well plate or a home built 96 well LED array made from 405 nm LEDs (12nm FWHM, ~20mW per well, SuperbrightLEDS and ExpressPCB) was used to uniformly photoactivate a 96-well plate (variation in photoactivation for a standard sample ~10% well-well). pK_a measurements were made using 100mM prepared buffers (Hampton Research). Gel filtration was performed using the Superdex 75 column (GE Healthcare) on the BioLogic LP purification system (BioRad). Molecular weight standards (GE Healthcare) and sample solutions were mixed together in gel filtration buffer (150mM Tris pH 7.5, 50mM NaCl), added to the column and eluted with 200 μL fractions collected into a well plate and 280nm absorbance, 480/510 fluorescence, and 560/580 fluorescence measured. Maturation kinetics were measured by mixing purified protein in denaturation buffer (8M Urea and 1mM DTT) and heating to 95C for 5

Nature Methods: doi:10.1038/nmeth.1296

minutes, diluted 100X into renaturation buffer (35mM KCl, 2mM MgCl2, 50mM Tris pH 7.5, 1mM DTT) and fluorescence monitored in the Tecan[13].

Mammalian Expression Vectors. All fluorescent protein fusion expression vectors were constructed using C1 and N1 (Clontech-style) cloning vectors. Kaede and KikGR were purchased from MBL International, and Dendra2 was purchased from Evrogen. EGFP was purchased from Clontech and mCherry was a gift of Roger Tsien (UCSD). wtEosFP and dEosFP were a gift from J. Wiedenmann (University of Ulm). To create cloning vectors, the appropriate FP was amplified with a 5' primer encoding an AgeI site and a 3' primer encoding either a BspEI (C1) or NotI (N1) site. The purified and digested PCR products were ligated into similarly digested EGFP-C1 and EGFP-N1 cloning vector backbones.

To generate fusion vectors, the appropriate cloning vector and an EGFP fusion vector were digested, either sequentially or doubly, with the appropriate enzymes and ligated together after gel purification. Thus, to prepare mEos2, tdEos, and Dendra2 N-terminal fusions (number of linker amino acids in parenthesis), the following digests were performed: chicken paxillin (22), EcoRI and NotI (Alan Horwitz, University of Virginia); human cytochrome C oxidase subunit VIII, BamHI and NotI (mitochondria, Clontech); rat α-1 connexin-43, EcoRI and BamHI (Matthias Falk, Lehigh University); human H2B, BamHI and NotI (George Patterson, NIH); N-terminal 81 amino acids of human β-1,4-galactosyltransferase, BamHI and NotI (Golgi, Clontech); human microtubule-associated protein EB3, BamHI and NotI (Lynne Cassimeris, Lehigh University); human vimentin, BamHI and NotI (Robert Goldman, Northwestern University); human keratin 18, EcoRI and NotI (Open Biosystems, Huntsville, AL);

Nature Methods: doi:10.1038/nmeth.1296

chicken paxillin, EcoRI and NotI (Alan Horwitz, University of Virginia); human zyxin, BamHI and NotI (Clare Waterman-Storer, NIH). To prepare C-terminal fusions, the following digests were performed: human β-actin, NheI and BglII (Clontech); human α-tubulin, NheI and BglII (Clontech); human light chain clathrin, NheI and BglII (George Patterson, NIH); human lamin B1, NheI and BglII (George Patterson, NIH); mouse VASP, NheI and BglII (Robert Fischer, NIH). Human vinculin cDNA was purchased from Open Biosystems (clone ID: 4520338) and installed in a Clontech-style plasmid using NheI and AgeI. The vector monomeric Kusabira Orange (mKO)-Vinculin was constructed by cloning into the NotI site of phKO1-MC1 (MBL, Intl.) using the oligos: 5'-GACTGCGGCCGCATGCCAGTGTTTCATACGCGCAC-3' and 5'-GATCGCGG CCGCCTACTGGTACCAGGGAGTCTTTCTAACC-3' with full-length vinculin cDNA template. After site-directed mutagenesis with the oligo 5'-CTAAGAGGGAGGTGGAA AATTCCGAGGATCCCAAGTTC-3', the plasmid pKO-VinculinRImut was obtained and used to prepare mEos2-Vinculin as previously described[14]. DNA for mammalian transfection was prepared using the Endonuclease-free Plasmid Maxi kit (QIAGEN).

Microscopy and Live Cell Imaging. All filters for fluorescence screening and imaging were purchased from Chroma Technology (Rockingham, VT), Omega Filters (Brattleboro, VT) and Semrock (Rochester, NY). HeLa epithelial (CCL-2, ATCC) and Grey fox lung fibroblast (CCL-168, ATCC) cells were grown in a 50:50 mixture of DMEM and Ham's F12 with 12.5% Cosmic calf serum (Hyclone) and transfected with Effectene (QIAGEN). Imaging was performed in Delta-T culture chambers (Bioptechs, Butler, PA) under a humidified atmosphere of 5% CO_2 in air. Imaging in widefield mode was performed with a Nikon (Melville, NY) TE-2000 inverted microscope equipped with

Nature Methods: doi:10.1038/nmeth.1296

Omega QuantaMax™ filters (QMax-Green and QMax-Red) and a Photometrics (Tucson, AZ) Cascade II camera or an Olympus (Lehigh Valley, PA) IX71 equipped with Semrock BrightLine™ filters (DAPI, 1160A; GFP-3035B; TIRTC-A) and a Hamamatsu (Bridgewater, NJ) ImagEM™ camera. Laser scanning confocal microscopy was conducted on a Nikon C1Si and an Olympus FV1000, both equipped with argon-ion (457 and 488 nm) and helium-neon or diode (543 and 561 nm, respectively) lasers and variable emission bandwidths (generally, 500-520nm for mEos2 green form and 560-590 nm for mEos2 red form). Spinning disk confocal microscopy was performed on an Olympus DSU-IX81 equipped with a Lumen 200 illuminator (Prior, Boston, MA), a Hamamatsu 9100-12 EMCCD camera, Semrock filters (GFP-3035B; TIRTC-A), and 10-position filter wheels driven by a Lambda 10-3 controller (Sutter, Novato, CA). In some cases, cell cultures expressing FP fusions were fixed after imaging in 2% *para*-formaldehyde (EMS, Hatfield, PA) and washed several times in PBS containing 0.05 M glycine before mounting with a polyvinyl alcohol-based medium. Morphological features in all fusion constructs were confirmed by imaging fixed cell preparations on coverslips using a Nikon 80i upright microscope and Semrock Filters (DAPI, 1160A; GFP-3035B; TIRTC-A) coupled to a Hamamatsu Orca ER or a Photometrics CoolSNAP™ HQ^2 camera.

Photobleaching Decay Kinetics. Widefield and laser scanning confocal microscopy photobleaching experiments were conducted with N-terminal fusions of the appropriate fluorescent protein to human histone H2B (6-residue linker) to confine fluorescence to the nucleus in order to closely approximate the dimensions of aqueous droplets of purified fluorescent proteins used in widefield measurements by the Roger Y. Tsien

Nature Methods: doi:10.1038/nmeth.1296

laboratory[15]. HeLa-S3 cells (ATCC; average nucleus diameter = 17μm) were transfected with the H2B construct using Effectene (QIAGEN) and maintained in a 5% CO_2 in Bioptechs Delta-T imaging chambers for at least 36 hours prior to imaging. The chambers were transferred to a Bioptechs stage adapter, imaged at low magnification to ensure cell viability, and then photobleached using a 40x oil immersion objective for confocal (Olympus UPlan Apo, NA = 1.00) or a 40x dry objective (Nikon Plan Fluorite, NA = 0.85) for widefield studies. Photoconversion was accomplished with a MOSAIC digital diaphragm system (Photonic Instruments, St. Charles, IL) using an ultraviolet excitation filter (365/20 nm) at a power level of 20 mW/cm^2 for 12 to 15 sec. A metal halide illumination source (EXFO) was subsequently used without neutral density filters for widefield photobleaching assays on each species (green and red). Output power at the objective focal plane was measured with a Newport 1918-C meter (Irvine, CA). For the green species of each optical highlighter, an Omega XF 100-2 filter set was used for photobleaching (~175 mW/cm^2 power), and for the red species, a Chroma TRITC HQ filter set was used (~475 mW/cm^2 power).

A 405-nm diode laser operating at a power level of 200 μW/cm^2 for 30-40 sec was used for photoconversion in the confocal assays. Laser lines (543 nm, He-Ne and 488 nm, argon-ion) were adjusted to an output power of 100 μW, measured with a FieldMaxII-TO (Coherent) power meter equipped with a high-sensitivity silicon/germanium optical sensor (Coherent OP-2Vis). The instrument (Olympus FV1000) was set to a zoom of 4X, a region of interest of 341.2 μm^2 (108 x 108 pixels), a photomultiplier voltage of 650 V, and an offset of 9% with a scan time of 0.181 seconds per frame. Nuclei having approximately the same dimensions and intensity under the

Nature Methods: doi:10.1038/nmeth.1296

fixed instrument settings were chosen for photobleaching assays. Fluorescence using the 543 laser was recorded with a 570 nm dichromatic mirror and 656 nm longpass barrier filter, whereas emission using the 488 laser was directly reflected by a mirror through a 510 nm longpass barrier filter.

In order to assure that fixed nuclear localization of histone H2B did not obscure photobleaching results, several controls using highly mobile nuclear fusions were examined in parallel. Fusions of mEGFP to histone H1 and heterochromatin protein 1 (HP1), both dynamically mobile proteins in the nucleus, exhibited photobleaching kinetics with corrected values within 5% of the range obtained with mEGFP-H2B.

The confocal photobleaching half-times were calculated as described[8] as the time required to reduce the scan-averaged emission rate to 50% from an initial emission rate of 1000 photons/s per fluorescent protein chromophore using the energy of a photon in Joules at the excitation laser wavelength and the extinction coefficient of the fluorescent protein at that wavelength. The average photon flux over the region of interest was then calculated and multiplied by the optical cross section of a fluorescent protein chromophore to achieve the scan-average excitation rate per fluorescent molecule. The time to bleach from an initial scan-average rate of 1000 photons/sec to 500 photons/sec was then calculated and normalized to an initial emission rate of 1000 photons/sec. For widefield experiments[15], the measured excitation filter and dichroic mirror transmission was used along with the spectral characteristics of the metal halide light source in this wavelength region to calculate the energy of each photon as a function of wavelength. Normalized photobleaching rates were then calculated as described[15] and presented as for confocal photobleaching rates in Supplementary Figure 11.

Nature Methods: doi:10.1038/nmeth.1296

References

1. Wiedenmann, J. *et al.*, *Proc. Natl. Acad. Sci. USA* **101**, 15905-15910 (2004).
2. Shroff, H. *et al.*, *Proc. Natl. Acad. Sci. USA* **104**, 20308-20313 (2007).
3. Gautier, I. *et al.*, *Biophys. J.* **80**, 3000-3008 (2001).
4. Deich, J., Judd, E.M., McAdams, H.H., and Moerner, W.E., *Proc Natl Acad Sci U S A* **101**, 15921-15926 (2004).
5. Creighton, T.E., *Proteins: Structures and Molecular Properties*, 2nd ed. (W.H. Freeman, 1992).
6. Bates, M., Huang, B., Dempsey, G.T., and Zhuang, X., *Science* **317**, 1749-1753 (2007).
7. Hess, S.T. *et al.*, *Proc. Natl. Acad. Sci. USA* **104**, 17370-17375 (2007).
8. Geisler, C. *et al.*, *Appl. Phys. A* **88**, 223-226 (2007).
9. Stiel, A.C. *et al.*, *Biophys J* **95**, 2989-2997 (2008).
10. Thompson, R.E., Larson, D.R., and Webb, W.W., *Biophys J* **82**, 2775-2783 (2002).
11. Kunkel, T.A., *Proc Natl Acad Sci U S A* **82**, 488-492 (1985).
12. Betzig, E. *et al.*, *Science* **313**, 1642-1645 (2006).
13. Reid, B.G. and Flynn, G.C., *Biochemistry* **36**, 6786-6791 (1997).
14. Shaner, N.C., Patterson, G.H., and Davidson, M.W., *J. Cell Sci.* **120**, 4247-4260 (2007).
15. Shaner, N.C., Steinbach, P.A., and Tsien, R.Y., *Nat Methods* **2**, 905-909 (2005).

Author contributions

L.L.L. designed mEos2 variants and S.M. generated and analyzed mEos2 variants and performed PALM imaging. M.W.D., K.L.H. and C.S.M. generated cloning vectors and fusion constructs, performed widefield, TIRF, and confocal microscopy, and conducted photobleaching experiments. S.M., M.W.D. and L.L.L. designed and planned the project and wrote the manuscript.

Nature Methods: doi:10.1038/nmeth.1296